Indian Journal of Engineering & Materials Sciences
Vol. 32, June 2025, pp. 379-393
DOI: 10.56042/ijems.v32i03.16101

Formulation and analysis of novel hybrid material for shock wave endurance with integrated image processing techniques

Pradeep Kumar Sulur Loganathan[a*] & Maniraj Jaganathan[b]

[a]KIT-Kalaignarkarunanidhi Institute of Technology, Department of Aeronautical Engineering Coimbatore 641 402, Tamil Nadu, India

[b]KIT-Kalaignarkarunanidhi Institute of Technology, Department of Mechanical Engineering Coimbatore 641 402, Tamil Nadu, India

Received: 31 December 2024; accepted: 23 March 2025

The growing demand for protective materials in high-stress environments, such as bomb squad suits, fire-resistant suits, and the oil and gas industry, has rendered their development more critical. Existing solutions have not succeeded in achieving a cohesive integration of structural integrity, thermal stability, and vibration dampening. This study addresses this gap by examining the shock wave penetration resistance of silica aerogel, sorbothane, and graphite composites. We used ANSYS to conduct simulations on the individual materials and six composite configurations to evaluate their mechanical properties in comparison. A high-pressure shock tunnel has been used to assess shock wave effects, while Scanning Electron Microscopy (SEM) has been utilised to examine the consequences on microstructure. Thermogravimetric Analysis (TGA), Differential Thermal Analysis (DTA), and image processing techniques have corroborated the results. The findings demonstrate that silica aerogel and graphite possess considerable strength, whereas sorbothane excels in vibration absorption. The SEM analysis indicates that their porous, clustered, and interplanar characteristics enhance their shock resistance. Combination 1 has shown superior performance among all composites, exhibiting excellent thermal stability under shock-inducing loads. This study demonstrates that the silica aerogel–sorbothane–graphite composite exhibits a synergistic equilibrium of mechanical strength, thermal resistance, and vibration attenuation, making it suitable for advanced protective applications.

Keywords: Graphite, Image processing techniques, Shock resistant materials, Silica aerogel, Sorbothane

1 Introduction

The utilization of shock waves is becoming more prevalent in innovative ways in the modern economy. The thermodynamic characteristics of hypersonic flow, such as pressure and temperature, are easily identifiable in any medium through which it travels[1]. The impressive capacity for expansion constitutes a noteworthy shift in paradigm[2]. The shock tube is widely acknowledged as a highly effective instrument for reflective shock waves measurement. The execution of this approach has resulted in the enhanced delineation of combustion mechanisms within the framework of design and simulation. For over 50 years, shock tubes have been widely employed to study physical and chemical phenomena at high temperatures[3]. The shock tube has emerged as a prominent research tool in the aviation industry, particularly in the post-World War II era[4]. Graphite structures lowers shockwave velocity as density increases. The stresses decrease dramatically as the atoms move freely away from the reflecting wall. Graphites' porosity allows for efficient energy absorption, making them suitable for shockwave applications[5]. The establishment's perspective ambit comprises various mechanical implementations, including the evaluation of structural impact and the study of shock-induced deformation in metals and composites, in addition to experiments concerning chemical kinetics and ignition delay for promising biofuels. These applications are widely regarded as being highly stimulating[6]. Shock tubes are widely regarded as a reliable instrument for investigating diverse phenomena, including the genesis and dissemination of shock waves, perception, and other related subjects. The apparent ease of its functionality has garnered the interest of several academics[7]. Shock tubes have been instrumental in investigating fast response kinetics and developing reaction systems for many years. The method comprises a membrane under reduced pressure, effectively separating the driver component, which contains a pressurized inert gas, from the driven segment that transports the test mixture. The experimental procedure begins with the rupture of the membrane,

*Corresponding author (E-mail: pradeepzero1991@gmail.com)

which results in the generation of an incident shock due to the pressure differential. The pressure within the driver compartment is gradually elevated until the diaphragm undergoes a rupture, producing a shock wave that travels through the gas being propelled. Upon the ingress of the shock front into the driven gas, no significant alteration in pressure is detected in either the driver or the driven regions. The interaction between the flow of the driven and driver gases occurs in a unidirectional manner, albeit at a lower velocity than that of the shock front in Fig. 1[8 - 10].

1.1 History of shock tubes

The visual representation in Fig. 2 illustrates the chronological advancement of shock tubes over the past century. Shock tubes have been widely utilized across diverse industries and academic disciplines, including but not limited to medicine, agriculture, manufacturing, and engineering.

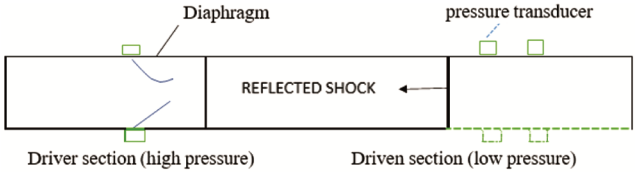

Fig. 1 — Schematic diagram of shock tube.

1.2 Shockwaves existing in nature

The shockwaves itself is a natural phenomena that exists as different forms in nature and this can be illustrated in the Table 1.

1.3 Research objective

Emerging technologies in aircraft industries, defence, and various other industries require materials that can tolerate intense temperature loads, high mechanical stress, and severe vibrating conditions without sacrificing performance or durability. Existing materials either lack sufficient thermal stability under shock-induced thermal loads or do not provide suitable vibration dampening, resulting in a major gap in the design of multifunctional composites. Combining the unique features of silica aerogel, sorbothane, and graphite allows for the creation of a material that achieves a combination of thermal endurance, mechanical strength, and vibrational absorption, so addressing the limits of typical single-material solutions.

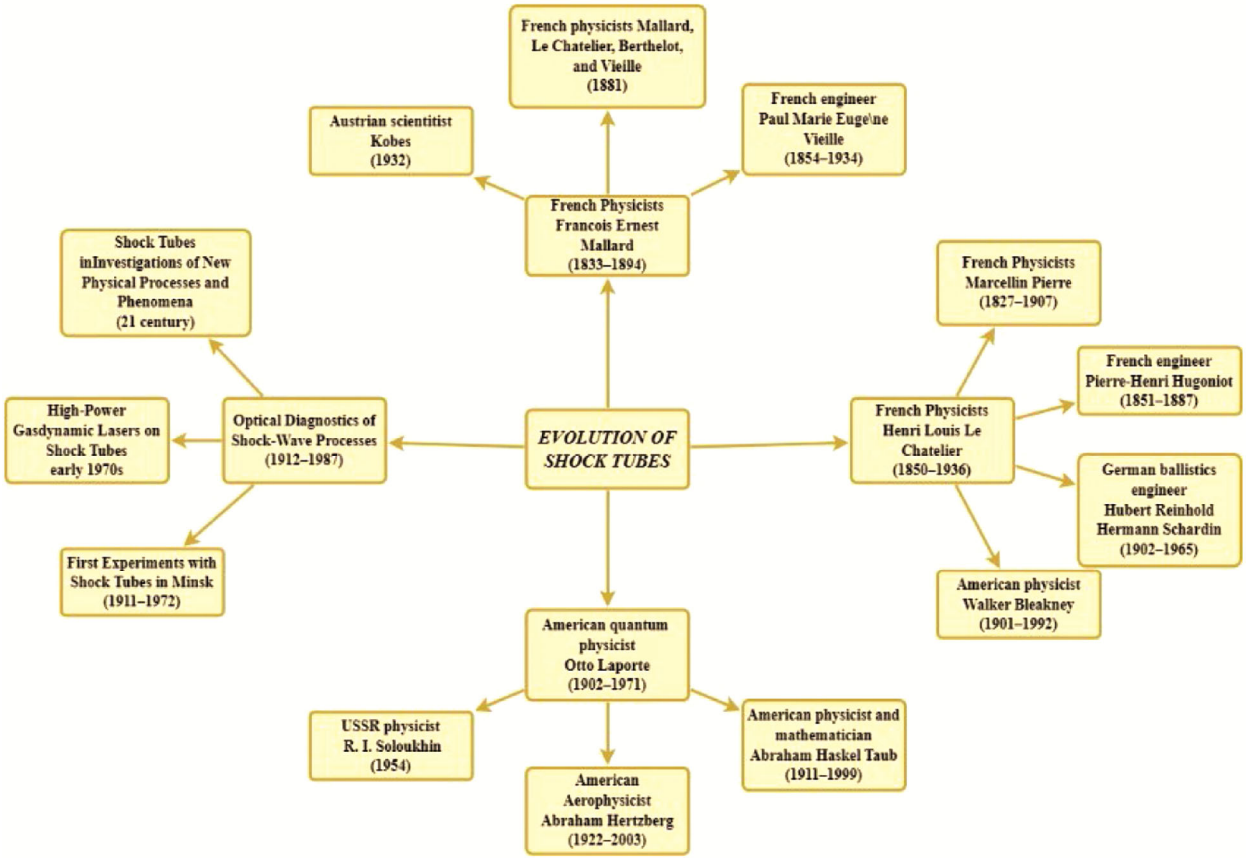

Fig. 2 — Evolution of Shock tubes in the research world.

Table 1 — Formation of shock waves in nature.

S.No	Shockwaves in Nature	Formation of Shock waves
1	Earthquakes	Seismic waves generated during an earthquake create shockwaves that travel through the Earth. The energy released during an earthquake causes the ground to shake, and these shockwaves can result in significant damage.
2	Thunderstorms	Lightning strikes during a thunderstorm create shockwaves, known as thunder. The rapid expansion of air due to the extreme heat of lightning generates a shockwave that we perceive as thunder.
3	Supersonic Flight	When an object, like an aircraft, travels faster than the speed of sound, it generates shockwaves known as sonic booms. These shockwaves result from the compression of air molecules as the object moves through the atmosphere.
4	Volcanic Eruptions	Explosive volcanic eruptions can produce shockwaves in the form of volcanic blasts and pyroclastic flows. The rapid release of gas and magma generates shockwaves that can cause destruction in the surrounding area.
5	Meteorite Impacts	When a meteorite enters the Earth's atmosphere and impacts the surface, it generates shockwaves due to the rapid deceleration and release of energy upon impact.
6	Ocean Waves	Large and powerful ocean waves, such as tsunamis, create shockwaves that can travel vast distances across the ocean. Tsunamis are typically caused by underwater earthquakes or volcanic eruptions.
7	Solar Flares	Explosive events on the Sun's surface, known as solar flares, can generate shockwaves in the form of coronal mass ejections (CMEs). These shockwaves consist of charged particles and electromagnetic radiation that can impact the Earth's magnetic field.
8	Shrimp Fish	It rapidly close their claws, producing shock waves in the water that paralyze fish, worms, and other prey. How a species evolved from gradual pinching to lightning-fast snapping remains a long-standing puzzle to scientists.

2 Materials and Methods

2.1 Shock wave penetration resistant materials

2.1.1 Silica aerogel

Silica aerogel is a magnificent material with excellent thermal insulation properties, a high surface area, and an extremely low density. It is known as the "lightest solid" or "frozen smoke" due to its low density and ethereal appearance[11]. The following are some of the primary features and applications of silica aerogel as shown in Fig. 3:

- ***Composition***- The major component of silica aerogel is silica (silicon dioxide), which is also found in glass and quartz. The gel is created using sol-gel technique, which generates a silica gel and removes the liquid component by supercritical drying[12].
- ***Low density***- Silica aerogel has a low density of 0.0011 g/cm³, making it very lightweight. It is therefore one of the lightest solid materials yet found[13].
- ***High surface area***- Because of its porous structure, it has an enormous surface area. Aerogels have a porous network that includes up to 99% empty space[14].
- ***Transparent***- Silica aerogel may be clear or translucent, depending on the manufacturing technique. This feature makes it useful for optics and as a lightweight alternative to glass[15].

Fig. 3 — Silica aerogel fabric.

2.1.2 Sorbothane

Sorbothane as shown in Fig. 4 is a viscoelastic polymer with superior damping and isolation qualities. It is well-known for its capacity to absorb and disperse energy, making it helpful in a variety of applications that need vibration and shock reduction[16].

- ***Viscoelasticity***- Sorbothane is viscoelastic which enables it to absorb and discharge energy effectively. It has significant damping properties, making it useful for decreasing vibrations and attenuating shock[17].
- ***Vibration isolation***- In electronics, sorbothane is often used to reduce vibration and shield sensitive parts from shocks. It is used in industrial settings

to reduce wear and tear and improve equipment efficiency by isolating vibrations in machines[18].

- ***Shock absorption***- Sorbothane is utilized to reduce impact forces and improve comfort in the design of insoles, shoe inserts, and other sports equipment. It is used in medical equipment and gadgets to reduce shocks and dampen vibrations[19].

2.1.3 Graphite

The element carbon exists in crystalline form as graphite. It is a naturally occurring mineral with a number of special qualities that help it work well in a variety of industrial settings as shown in Fig. 5.

- ***Thermal conductivity***- Graphite also has a high thermal conductivity, which allows it to effectively transmit heat. This feature makes it useful in applications like as heat exchangers, thermal management systems, and crucibles in high-temperature operations[20].
- ***Chemical stability***- At standard temperatures and pressures, graphite does not react with most chemicals or gases due to its relative chemical inertness. This qualifies it for use in equipment used in chemical processing as well as corrosive conditions[21].
- ***High melting point***- Graphite has a high melting point of around 3,600°C (6,512°F), making it appropriate for use in high-temperature applications such as refractory materials, crucibles, and furnace linings[22].
- ***Softness and flexibility***- Graphite is rather soft and flexible, despite its hardness and endurance. This characteristic makes it simple to machine, shape, and mold into a variety of shapes and forms, such as pencils, crucibles, and metal casting molds[23].

The Mechanical properties of materials taken in the investigation properties are mentioned in Table 2.

2.2 Shockwaves generation in the shock tunnel for investigation

The materials were prepared in standard sample sizes and mounted securely within the shock tube chamber as shown in Fig. 6. Controlled shock

Fig. 4 — Sorbothane rubber.

Fig. 5 — Graphite sheet.

Table 2 — Mechanical properties of insulating materials.

Mechanical properties	Silica Aerogel	Graphite	Sorbothane
Density	100 kg/m^3	2260 kg/m^3	1370 kg/m^3
Bulk modulus	-	-	4.5 N/m^2
Specific surface Area	500-950 m^2/g	1.3-90 m^2/g	-
Modulus of Elasticity	106-107N/ m^2	11.5 GPa	-
Temperature range	300 to 1000 ºC	150 to 650 ºC	-20 to + 140 ºC
Compression stress	2 MPa – 4.2 MPa	20 to 220 MPa	10 MPa
Tensile strength	16 KPa	14 MPa	0.520 MPa
Melting point	1200 ºC	3600 ºC	>93 ºC
Thermal conductivity	0.013 W/m-k	200 W/m-k	0.370 W/m-k
Electrical Conductivity	40 GHz	10 GHz	8.75 GHz
Heat Capacity	1900 J/gK	720 J/g K	-

waves were generated, simulating real-world conditions such as high-pressure pulses and rapid thermal loads. Subsequent analyses were conducted to evaluate material deformation, fracture patterns, and microstructural changes, providing insights into their performance and suitability for advanced thermal and structural applications.

The partial vacuum established in the operated region before to the explosion must cause the pressure of the driven gas to be much lower than the surrounding environment in order to produce high-pressure shockwaves. A sample is transferred to the testing area after the driving component has been cleaned. Shock waves are released onto the specimen, which is positioned in the test section seen in Fig. 6, when the diaphragm ruptures, as illustrated in Fig. 7. The ensuing exposure is then examined using SEM and TGA techniques. The shock tunnel used for testing is shown in Fig. 8.

3 Results and Disscusion

3.1 Effects on strength and hardness

The structural response of the Silica aerogel, Sorbothane, and graphite are analyzed through static structural analysis in ANSYS to calculate the stresses, strains, and pressures imposed on the above materials by the impact shock waves, which are to be considered as pressure forces. These three materials were subjected to three different pressure loads, 3.5, 4.5, and 5.5 bar. The amount of stress imposed on the silica aerogel, Sorbothane, and graphite is shown in the Figs 9, 10 & 11 and the observations are

Fig. 6 — Test specimen.

Fig. 7 — Busted diaphragm.

Fig. 8 — Shock tunnel setup at karunya university in coimbatore, Tamil Nadu.

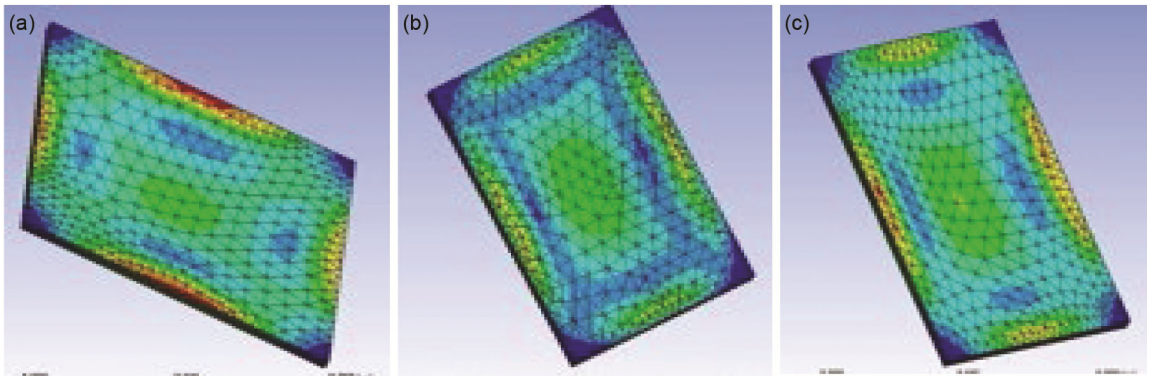

Fig. 9 — Equivalent stress (Von-Mises) (a) silica aerogel, (b) sorbothane and (c) graphite at 3.5 bar.

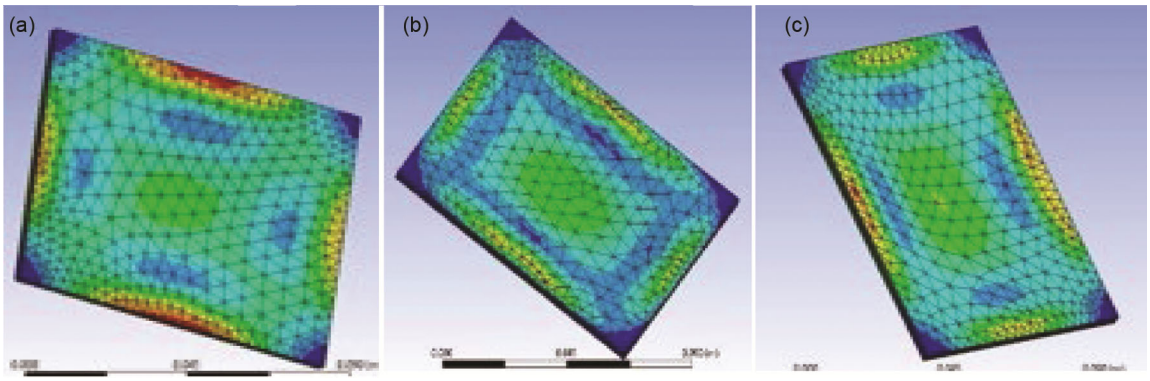

Fig. 10 — Equivalent stress (Von-Mises) (a) silica aerogel, (b) sorbothane and (c) graphite at 4.5 bar.

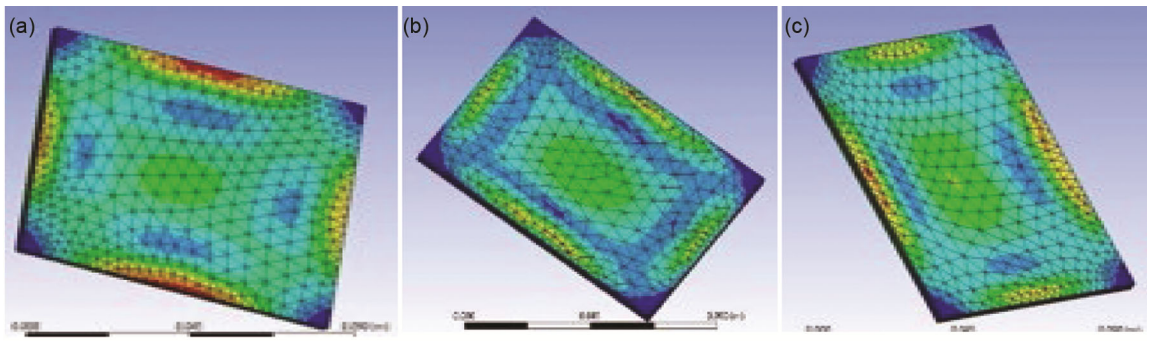

Fig. 11 — Equivalent stress (Von-Mises) (a) silica aerogel, (b) sorbothane and (c) graphite at 5.5 bar.

At 3.5 bar, Sorbothane can withstand a maximum stress of 7.8149×10^7 Pa, while at 4.5 bar, silica aerogel can endure a maximum stress of 9.8828×10^7 Pa. At 5.5 bar, graphite demonstrates its strength by withstanding a maximum stress of 1.1663×10^8 Pa. Notably, silica aerogel exhibits high average and minimum stress values across all tested pressures of 3.5, 4.5, and 5.5 bar represented in the Table 3. Furthermore, silica aerogel stands out for its exceptional ability to sustain the applied stress over a prolonged period compared to Sorbothane and graphite, highlighting its superior resilience under extreme conditions

4.2 Effects on ductility

The deformation characteristics of Silica aerogel, Sorbothane, and Graphite at different pressure has shown in the Figs 12, 13 and 14.

The results of the deformation analysis have shown in the Table 4, and the observations at pressures 3.5, 4.5, and 5.5 bar. The silica aerogel has high maximum and average deformation values, which means that silica aerogel will deform more when compared to Sorbothane and graphite. Graphite has the second-highest maximum and average deformation values, which means that graphite will deform more when compared to Sorbothane. Sorbothane has the most

Table 3 — Equivalent stress (von-Mises).

Pressure Range	Material	Minimum Stress (Pa)	Maximum Stress (Pa)	Average Stress (Pa)
3.5 bar	Silica Aerogel	1.3789×10^{5}	7.6866×10^{7}	2.3267×10^{7}
3.5 bar	Sorbothane	12685	7.8149×10^{7}	1.6255×10^{7}
3.5 bar	Graphite	99270	7.4218×10^{7}	2.0135×10^{7}
4.5 bar	Silica Aerogel	1.7728×10^{5}	9.8828×10^{7}	2.9914×10^{7}
4.5 bar	Sorbothane	16309	1.0048×10^{8}	2.09×10^{7}
4.5 bar	Graphite	1.2763×10^{5}	9.5423×10^{7}	2.585×10^{7}
5.5 bar	Silica Aerogel	2.1668×10^{5}	1.2079×10^{8}	3.6562×10^{7}
5.5 bar	Sorbothane	19933	1.2281×10^{8}	2.5544×10^{7}
5.5 bar	Graphite	1.56×10^{5}	1.1663×10^{8}	3.1595×10^{7}

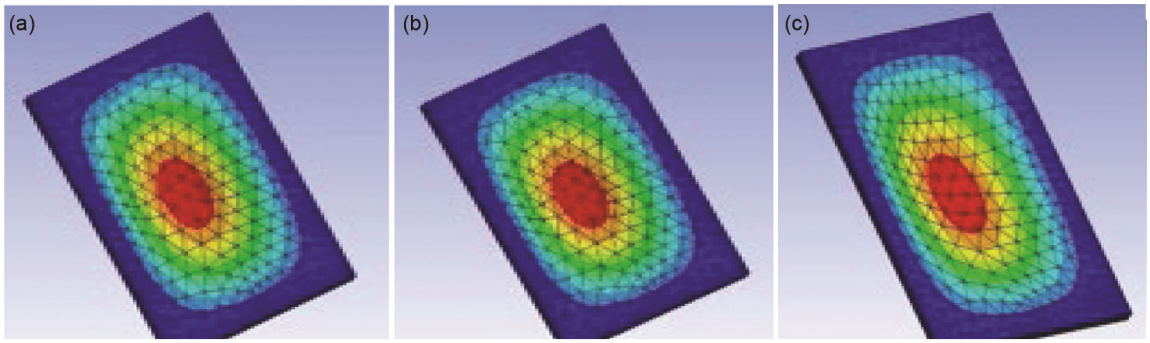

Fig. 6 — Deformation (a) silica aerogel, (b) sorbothane and (c) graphite at 3.5 bar.

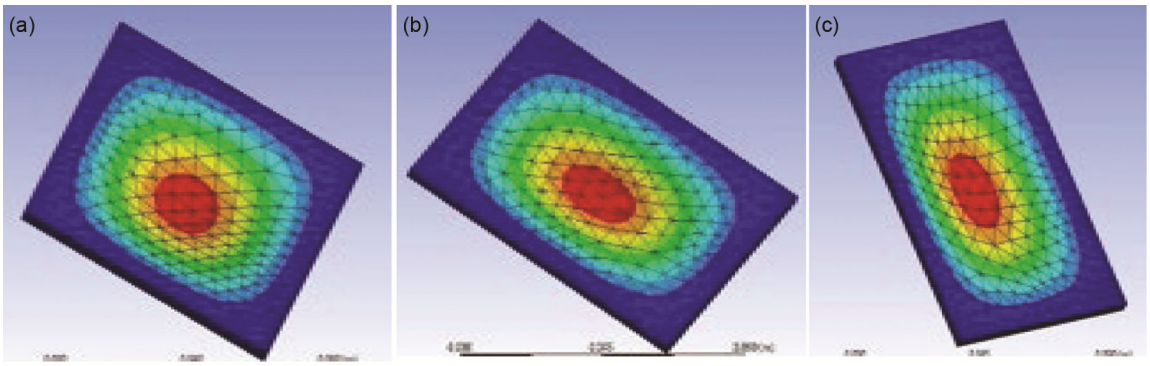

Fig. 7 — Deformation (a) silica aerogel, (b) sorbothane and (c) graphite at 4.5 bar.

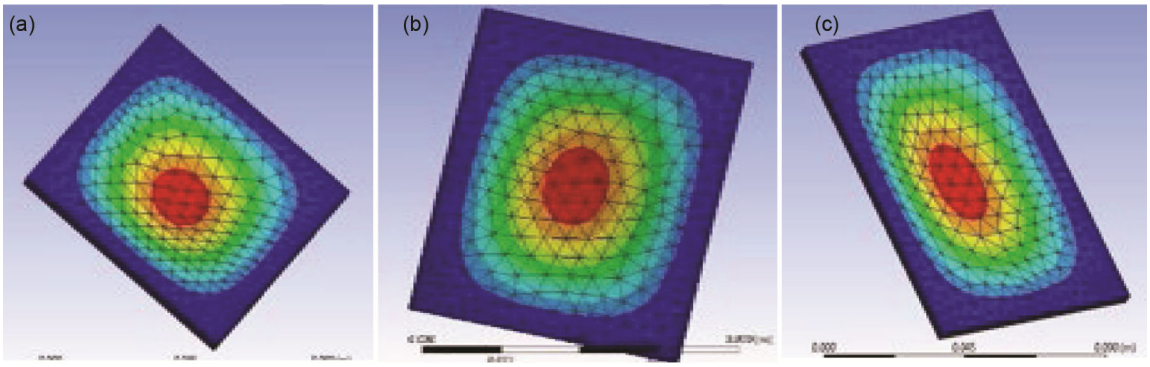

Fig. 8 — Deformation (a) silica aerogel, (b) sorbothane and (c) graphite at 5.5 bar.

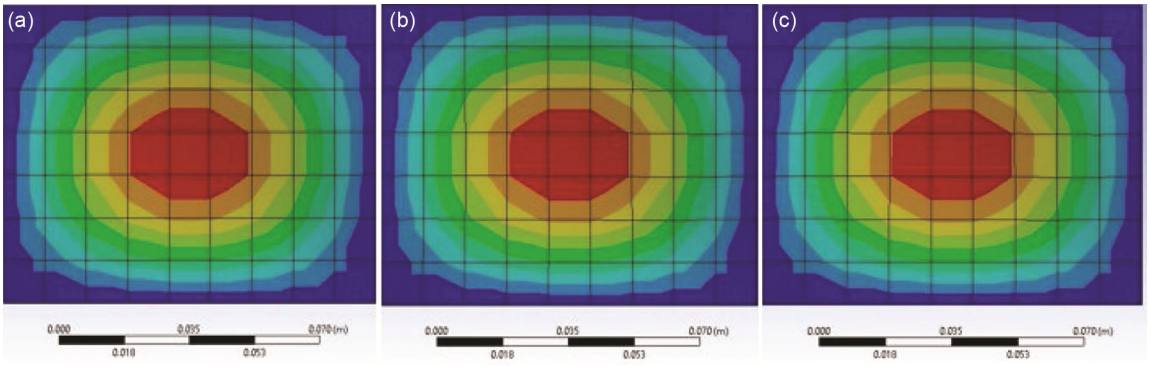

Fig. 9 — Total deformation patterns (a) silica aerogel, (b) sorbothane and (c) graphite.

Table 4 — Resultant deformation of the materials.

Pressure Range	Material	Minimum Deformation (Pa)	Maximum Deformation (Pa)	Average Deformation (Pa)
3.5 bar	Silica Aerogel	0.009676	1.0589×10^{5}	14454
3.5 bar	Sorbothane	0.007241	8.817×10^{-2}	1.382×10^{-2}
3.5 bar	Graphite	0.02242	0.20184	3.4169×10^{-2}
4.5 bar	Silica Aerogel	18488	9.8828×10^{7}	2.9924×10^{7}
4.5 bar	Sorbothane	0.02142	0.11336	1.7769×10^{-2}
4.5 bar	Graphite	0.02885	0.25951	4.3931×10^{-2}
5.5 bar	Silica Aerogel	36977	1.6639×10^{5}	27428
5.5 bar	Sorbothane	0.01523	0.13855	2.1718×10^{-2}
5.5 bar	Graphite	0.03524	0.31718	5.3693×10^{-2}

minor maximum and average deformation values, which means that Sorbothane will deform less when compared to silica aerogel and graphite.

4.3 Effects on vibration resistance

The vibration characteristics of Silica aerogel, Sorbothane, and Graphite at different pressure has shown in the Fig. 15.

The results of the deformation analysis have shown in the Table 5, and the observations at pressures 3.5, 4.5, and 5.5 bar. Silica aerogel has a deformation at a minimum frequency of 0.36963 Hz, which means that silica aerogel will get deformation (40.202mm) even at the minimum vibration level. Compared to silica aerogel, Sorbothane has an average frequency value of 104.17 Hz, which means that Sorbothane can withstand minimal vibration. Graphite has extraordinary vibration resistance ability with a frequency value of 6652.3 Hz, which means that graphite will get minimum deformation of 1005.6mm even at high frequency compared to the other two materials.

4.4. Effects of Stress on Composite Materials:

If a material is malleable, its equivalent stress might serve as an indicator of its overall quality. Engineers need this only number to determine whether or not a material has surrendered. The results of the von-mises analysis have given in the Table 6, The observations are

- Combination 1 & 5 shown in Fig. 16 (a & e) shows that this hybrid combination will have a high elasticity and factor of safety.

Table 5 — Results of modal analysis.

Material	Total Deformation (mm)	Frequency (Hz)
Silica Aerogel	40.202	0.36963
Sorbothane	10.869	104.17
Graphite	1005.6	6652.3

Table 6 — Equivalent stress analysis for hybrid combinations.

Combinations	Maxi. Stress (N/mm^2)	Min. Stress (N/mm^2)
Combination: 1 (silica aerogel, Sorbothane, graphite)	0.133×10^{12}	538937
Combination:2 (Sorbothane, graphite, silica aerogel)	0.128×10^{12}	228086
Combination: 3 (graphite, silica aerogel, Sorbothane)	0.722×10^{11}	0.461×10^{10}
Combination: 4 (silica aerogel, graphite, Sorbothane)	0.128×10^{12}	228086
Combination:5 (graphite, Sorbothane, silica aerogel)	0.133×10^{12}	538937
Combination: 6 (Sorbothane, silica aerogel, graphite)	0.722×10^{11}	0.461×10^{10}

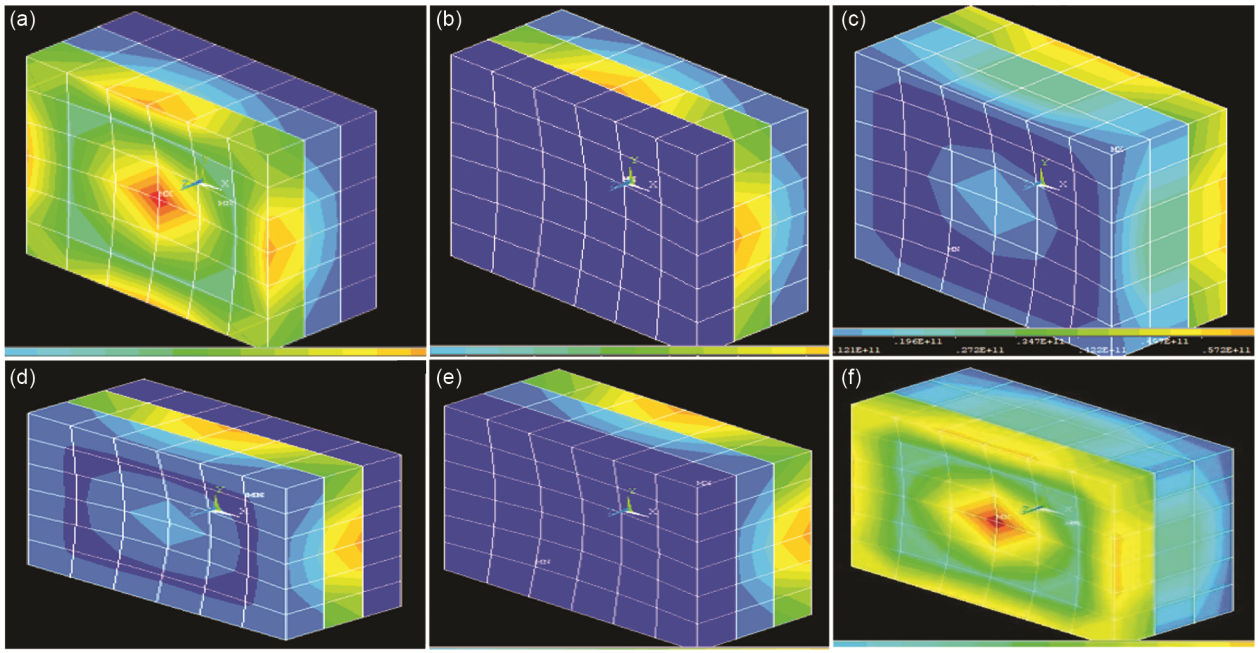

Fig. 16 — Resultant stress distribution of hybrid combinations (a) [silica aerogel, sorbothane , graphite], (b) [sorbothane, graphite, silica aerogel], (c) [graphite, silica aerogel, sorbothane], (d) [silica aerogel, graphite, sorbothane], (e) [graphite, sorbothane, silica aerogel] and (f) [sorbothane, silica aerogel, graphite].

- Combinations 2 & 4 shown in Fig. 16 (b & d) shows that this hybrid combination will also have good elasticity and factor of safety.
- Combinations 3 & 6 shown in Fig. 16 (c & f) shows that this hybrid combination will have moderate elasticity and a safety factor.
- The exciting factor is that in combinations 1 & 5, Sorbothane was placed as the intermediate material between silica aerogel and graphite. It illustrates that keeping Sorbothane as layer two will have the tremendous stress-tolerating ability and resist the penetration of stress quantity beyond it.
- In combinations 2 & 4, graphite was placed as the intermediate material between silica aerogel and Sorbothane. It illustrates that keeping graphite as layer two will have an admirable stress-tolerating ability and resist stress penetration quantity.

In combinations 3 & 6, silica aerogel was placed as the intermediate material between graphite and Sorbothane. It illustrates that keeping silica aerogel as layer two will have a moderate stress-tolerating ability and stress penetration resistance.

4.5 Effects of boundary layer interactions

The impact of shock waves on the material silica aerogel, sorbothane, graphite and combination silica aerogel-sorbothane-graphite has been conducted with a shock tunnel at Karunya University, Coimbatore. The specimen were kept at the test section where the shock waves hits the specimen. There are two pressure transducers placed after the diaphragm to measure the normal and reflected shock waves.

The shocktunnel results were validated from the oscilloscope data. Finding the first clear spike in the data that resulted in a crest in the peaks allowed for the computation of the shock wave passages. The first sensor were palced after the diaphragm and the second sensor were palced at the end wall section. In the oscilloscope display the yellow colour (first sensor) represents the normal shockwave and the green colour (second sensor) represents the reflected shockwaves. The impact of shockwave behavior in the Table 7 was discussed below. The diaphragm of the silica aerogel ruptures at a pressure of 13.9 bar, as seen in Fig. 17a. The yellow wave exhibits its first peak at 22mV, indicating the occurrence of an upstream normal shock with a velocity timing of 378 ms. The green color stays consistent until the normal shock waves are reflected upon impact with the silica aerogel specimen. The reflected wave peaks at 66.25mV with a velocity timing of 720 ms. From the picture, it can be noted that the reflected shock wave downstream (shown by the green color) has an impact on the normal shock, causing it to reach a second peak immediately after the first peak finishes. Figure 17b shows that the graphite diaphragm breaks when subjected to a pressure of 10.1

Table 7 — Characterstics of shockwave impact.

Materials	Diaphragm breaking pressure	Normal shock	Reflected shock	Normal shock velocity Timings	Reflected shock velocity Timings
Silica Aerogel	13.9 bar	22mV	66.25mV (8bar)	378 micro sec	720 micro sec
Graphite	10.1 bar	20mV	60.625mV (7.1 bar)	398 micro sec	696 micro sec
Sorbothane	7.2 bar	16.250mV	47mV (5.6 bar)	422 micro sec	698 micro sec
Combination 1 (silica aerogel, Sorbothane, graphite)	7.8 bar	15.6 mV	56.25mV (6 bar)	420 micro sec	710 micro sec

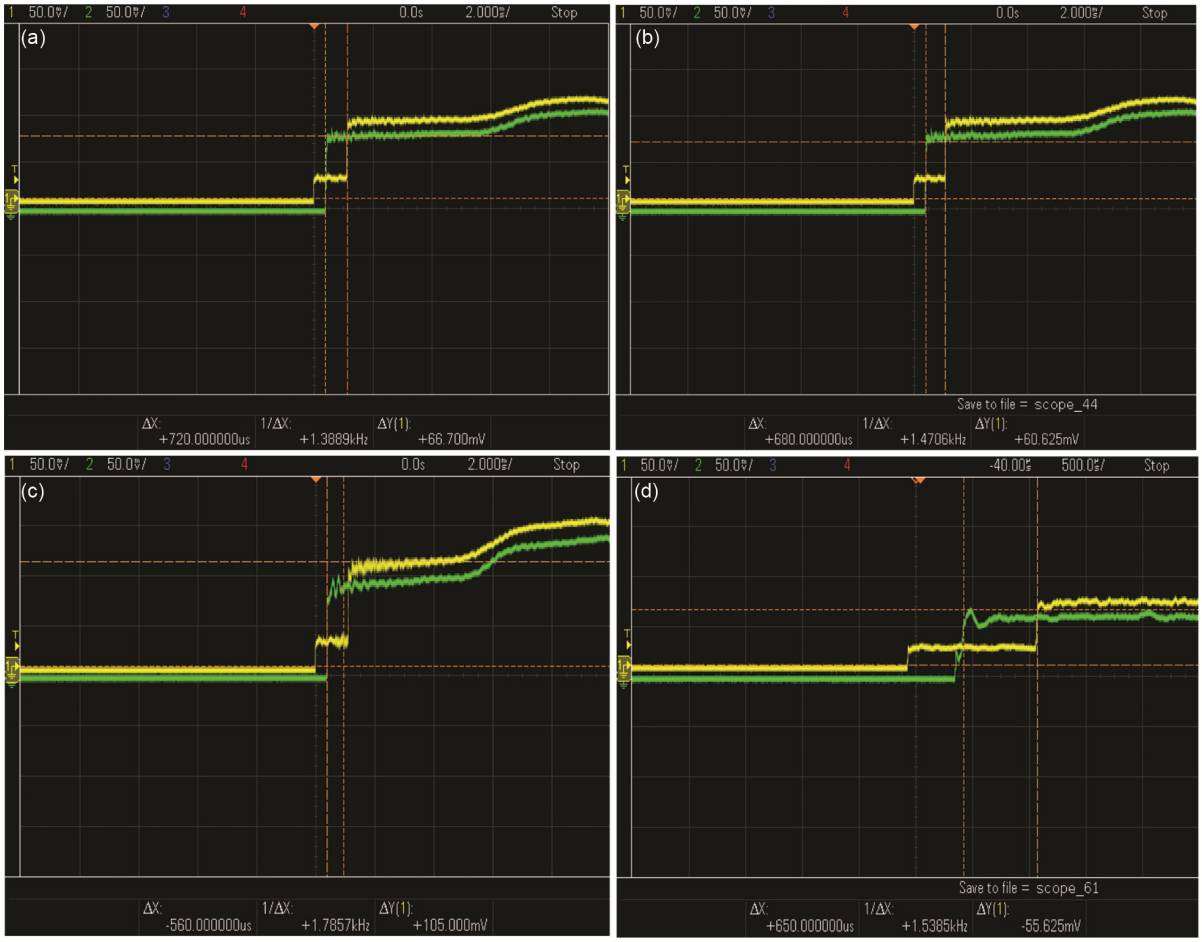

Fig. 17 — Boundary layer interaction due to Reflected shock waves.

bar. The amplitude of the normal shock reaches a maximum of 20 millivolts with a velocity timing of 398 milliseconds, while the reflected shock reaches a maximum of 60.25 millivolts with a velocity timing of 696 milliseconds. Additionally, the second peak of the usual shock happens immediately in this case.

According to Fig. 17c, the sarbothene diaphragm breaks when exposed to a pressure of 7.2 bar. The normal shock has a maximum amplitude of 16.25 mV and occurs at a velocity timing of 422 ms. On the other hand, the reflected shock has a maximum amplitude of 47 mV and occurs at a velocity timing of 698 ms. Furthermore, the second peak of the typical shock occurs immediately in this particular instance. Based on Fig. 17d, the combination 1 diaphragm fails when subjected to a pressure of 7.8 bar. The amplitude of the normal shock reaches a maximum of 15.6 millivolts and occurs at a velocity time of 420 milliseconds. Conversely, the reflected shock reaches its highest intensity at 56.25 millivolts and happens at a velocity time of 710 milliseconds. In addition, the second peak of the normal shock comes immediately in this specific case.

The experimental findings indicate that the combination 1 (silica aerogel-Sorbothane-graphite) exhibits superior resistance to shockwave impacts

compared to the individual components. This phenomenon is evident in the outcome shown in Fig. 17d, where the peak of the reflected shock wave has extended beyond the midpoint of the initial normal shock wave peak 1, in contrast to separate materials. The silica aerogel-Sorbothane-graphite combination is subjected to shockwaves with an input pressure of 7.8 bar. These shockwaves are reflected from the specimen at a pressure of 6 bar, indicating that only 1.8 bar pressure shock waves are absorbed by the specimen. The remaining are reflected back with a weak shock waves, resulting in a a smooth pulse formation. The intensity of the reflected shockwave diminishes after the kinetic pressure of the shock wave reaches equilibrium with the compressive pressure exerted by the combination of silica aerogel, Sorbothane, and graphite.

4.6 Image processing by CNNs for structural tranformations

The comparative study of the image charcterstics of the materials analysed using ANSYS can be done with Convolutional Neural Network (CNNs) using Lobe machine learning software. Lobe is equipped with simple instructions, making it accessible to users of all skill levels, without the need for coding or prior knowledge[24]. The simulation images were used as a data collection for image training to perform data processing by the lobe software.

Table 8 displays the image processing results obtained using the lobe program. In this context, the testing process involves identifying the resemblance between the images obtained from the ANSYS results. The comparison of image processing data for the structural and deformation analysis of silica aerogel, graphite, and sarbothene materials reveals a 50% correlation in their stress patterns. This indicates that their stress patterns match to a certain extent. Conversely, the remaining 50% of the data shows that their load carrying capacities differ when tested individually. The findings reveal a perfect agreement when testing structural-combination (1-6) and deformation-combination (1-6). This demonstrates that the combination (1-6) matches the stress distribution of the particular material. The findings show that combination materials have greater load-withstanding capabilities than individual materials.

Table 8 — Results of training model.

S. No	Image Processing	Similarites percentage (%)
1.	Structural - Deformation	50%.
2.	Structural – Combination (1-6)	100%.
3.	Deformation – Combination (1-6)	100%.

4.7 Morphological analysis

The combination 1 by keeping silica aerogel and graphite as target bodies studied at SRM Institute of Science and Technology in Chennai, Tamil Nadu. The electron gun cathode of a scanning electron microscope with an accelerating voltage of 1kV to 30kV provides topographical and elemental information at magnifications ranging from 10x to 300,000x, narrower probing beams at low and high electron energy, and clearer, less electrostatically distorted images with spatial resolution down to 1.5 nm.

The structural framework of silica aerogel is typically composed of silica, in which the liquid filled pores have been replaced with gas. In this structure the volume of silica is only 3% and the remaining 97% of the volume is air. These characteristics make aerogel the world's lowest density solid and most effective thermal insulator[25]. The microstructural studies using FESEM with 100 µm - 500x magnification exhibits that solid component in silica aerogel consists of 3D tiny intertwined clusters shown in the Fig. 18a. This orientation makes the air has very little room to move, inhibiting both convection and gas-phase conduction[26]. The magnification of 650x - 100 µm represents air voids shown in the Fig. 18b actually it not voids occurs in other materials instead in which the liquid has been replaced with air or gas in that voids. This results in an extremely low-density solid that can be imparted with several remarkable properties such as hydrophobicity[27]. The magnification of 1200x - 50 µm represents the formation of air gaps due to the impact of shockwaves on silica aerogel shown in the Fig. 18c. The shockwaves induces shear stress on the silica aerogel structure which forms cracks but the preponderance of air in an aerogel's structure fills that cracks which appears as air voids. The high gas content of Aerogels also gives them a variety of unique properties, including extremely low density, very low thermal conductivity, and very high porosity[28].

The magnification of 1500x - 50 µm represents the discontinuous cross linked fibre as shown in the Fig. 18d. The discontinuity is because of the impact of shockwaves on the fibre. The cross linked structure makes the silica aerogel to retains its shape in high-temperature settings, does not crack, clump and sag like other insulating materials. Because of this special

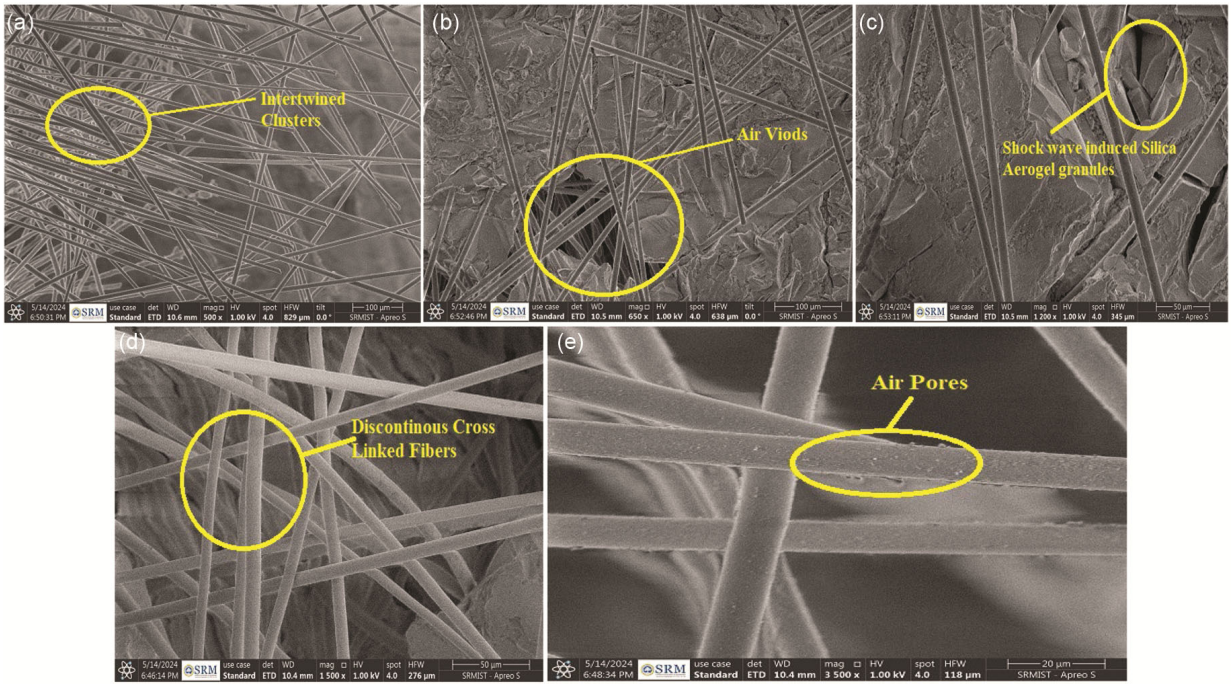

Fig. 18 — Microscopic view of silica aerogel blanket at magnification (a) 500x, (b) 650x, (c) 1200x, (d) 150x and (e) 3500x.

structure the material withstands the impacts of the shockwaves[29]. The magnification of 3500x - 20 µm represents the air pores as shown in the Fig. 18e. The air in the micropores occupies the major volume in the silica aerogel structure. The high air pores lowers the heat flow rate through the materials and makes it a hydrophobic nature. This extremely water repellent characters make the silica aerogel to withstands temperatures up to 1100 °F as well as offers the same quality insulation with 1/3 the thickness of other insulating materials[30].

The microstructure of the graphite revelas that it has a layered similar to flake structure shown in the Fig. 19a with the magnification of 5000x - 10 µm . This states that the graphite is a multilayer structure with closely overlapped to each other. The labelled area indicates to a location where the material shows thin, flat sheets; these flakes may imply layer separation or exfoliation, which is prevalent in materials like graphene ansd certain polymeric structures[31]. After the impacts of shockwaves on the graphite there is an material exfoliation as shown in the Fig. 19b with the the magnification of 10000x - 5µm. The shockwave strikes appear to have peeled the graphite layer off the surface, indicating material exfoliation. The irregular rough texture and the visible gaps between layers are the indications of the shock wave impacts. The flake like structure creates the ability to withstand the impacts of shockwaves to greater extent[32].

The interpalnar spacing that occurs in the graphite is shown in the Fig. 19c with the the magnification of 25000x - 3µm. The highlighted region exhibits apparent gaps between layers, which correspond to the spacing between planes of molecular sheets caused by shock waves. But the appearance of interpalanar spacing around the graphite sturucture is minimum which represents that the graphite can withstand the shock wave impacts[33]. The weak interlayer bonding in the graphite is shown in the figure. 19d with the magnification of 50000x - 1µm. The weak interlayer is due to the the weak van der Waals forces between layers which allows the graphite layer to get slide past for separation. Despite of weak van der Waals forces graphite structure has sufficiently strong attraction prevented the complete formation of individual graphene layers during the impacts of shock waves[34]. The SEM image highlights the interplanar spacing in a material that likely has a layered structure, such as graphene, graphite, or a similar material. The observed morphology suggests that the layers are being separated or exfoliated, a process that is useful for producing materials with high surface area and unique thermal and mechanical properties which makes the graphite a suitable material to withstand the impacts of the shock waves.

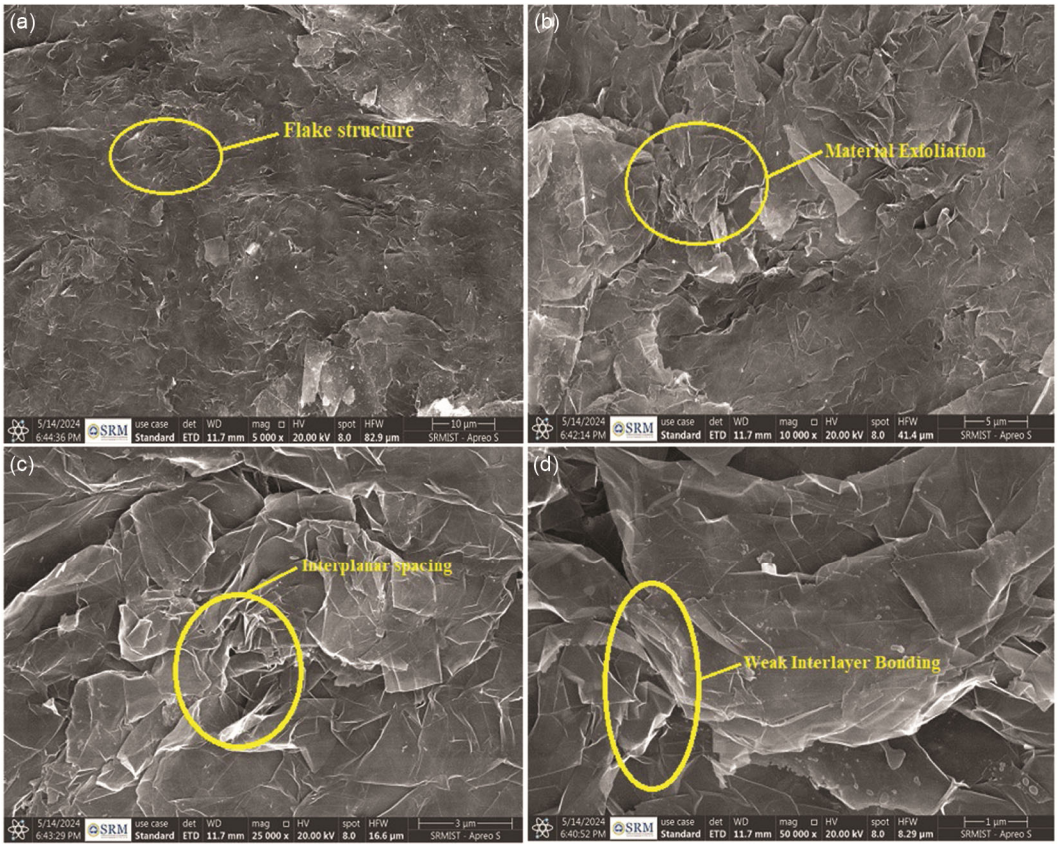

Fig. 19 — Morphplogical view of graphite sheet at magnification (a) 5000x, (b) 10000x, (c) 25000x and (d) 50000x.

4.8 Degradation temperature

A Thermogravimetric Analysis (TGA) graph as shown in Fig. 20, depicts the weight loss behaviour of a SiAG (silica aerogel-graphite) material after being exposed to shockwave impact. The x-axis depicts the temperature (°C), and the y-axis reflects the percentage of the sample's weight that remains. In the initial region up to ~200°C, the weight remains reasonably steady after that stability implies first minimal weight loss of 1% at lower temperatures, which might indicate that absorbed moisture in this dring stage. The loss of weight is due to the less moisture during the impacts of shock waves. Second weight loss is between ~200°C and 400°C is 6.7% due to the multi-step degradation process in a pyrolytic stage[35]. This stage is the evident for multi-step degradation of the temperature and also indicates the temperature withstanding ability of a material. The third weight loss is around 600°C to 700°C, there is a notable weight reduction of approximately 2.2% in this region. This loss could be associated with the decomposition of certain inorganic compounds and minor structural changes in the material due to the impact of shock waves on the material[36]. During the

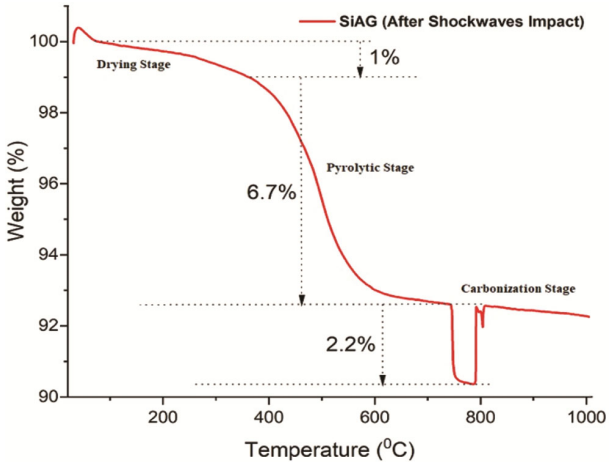

Fig. 20 — Degradation temperature.

shock wave impact the temperature get increases and due to this high temperature rise there is an evident of weight loss. The final region beyond 800°C is known as carbonization stage, following considerable decreases, the weight stabilises, suggesting that most decomposable components have been depleted. The remaining weight corresponds to the stable, non-volatile residue, which is most likely made up of stable temperature.

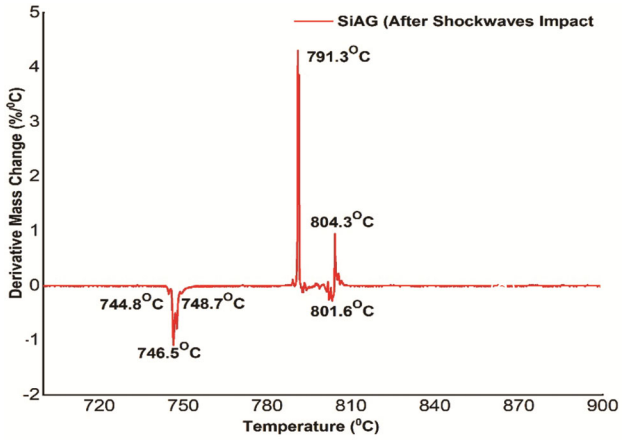

Fig. 21— Derivative mass change graph

Fig. 21, represents a Differential Thermal Analysis (DTA) for a silica aerogel-graphite (SiAG) sample after being impacted by shockwaves. The x-axis shows the temperature (°C), while the y-axis indicates the derivative mass change (%/°C). The graph shows a small negative peak at the temperature range 744.8°C to 748.7°C, indicating a minor mass loss in the drying stage. This could indicate a structural transformation, such as the partial oxidation of the residual graphite component and the release of trapped volatiles inside the silica aerogel matrix. There is a sharp positive peak at 791.3°C, a prominent peak indicates a significant exothermic reaction at the pyrolytic stage[37]. In this stage the silica aerogel-graphite sample undergoes several temperature transitions due to the impacts of shock waves, as a result the majority of which are caused by graphite oxidation and probable phase shifts in the silica matrix[38]. The two small peaks are observed at the temperature range of 801.6°C to 804.3°C in a carbonization stage, suggesting minor exothermic reactions with structural transitions in the material. These could be attributed to phase changes in the silica aerogel matrix and further oxidation of residual carbon content possibly influenced by the impact of shockwaves that altered the structural properties of the composite. After the final peak, the curve flattens, indicating that the major thermal events have ended. At this phase, the temperature rise due to the impacts of shock wave are settle down and the material is likely composed of non-oxidizable as well as stabilization beyond 810°C.

4 Conclusion

This study demonstrates that the silica aerogel–Sorbothane–graphite composite is a promising multifunctional thermal barrier material due to its unique combination of structural integrity, thermal stability, and vibration attenuation. The structural analysis indicated that silica aerogel and graphite enhanced the strength of the structure, while Sorbothane effectively dampened vibrations. Shock wave impact testing, in conjunction with SEM analysis, demonstrated that silica aerogel and graphite can withstand dynamic loading, while TGA–DTA investigations indicated that the composite has significant stability at elevated temperatures. Composite 1 had superior performance compared to all other evaluated formulae. It surpassed the others by integrating mechanical strength, vibrational dampening, and heat resistance in a cohesive manner. The findings have significant ramifications for enterprises operating in very adverse environments. The composite's balanced attributes provide it an excellent option for advanced thermal protection systems, particularly in aviation re-entry vehicles, fire-resistant protective apparel, and safety applications within the oil and gas sector. The study highlights the significant potential of hybrid material systems that intentionally include aerogels, viscoelastic elements, and carbon-based reinforcements to overcome the limitations of conventional thermal barriers. This work primarily contributes by demonstrating the feasibility and performance advantages of hybrid composites via comprehensive experimental validation. Future research should focus on improving manufacturing methods, optimising component ratios for particular applications, and assessing long-term durability under cyclic thermal and mechanical stresses. Prototyping and field testing in aviation and industrial protection systems will be crucial for transitioning this material from the laboratory to practical use.

References

1 Zhang C, Dong Y & Ye C, *Adv Eng Mater*, 23 (2021) 1-24.
2 Aganin A A & Mustafin I N, *Int J Multiph Flow*, 144 (2021) 103792.
3 Fregonese S, *Conflict Soc*, 7 (2021) 26-41.
4 Zhang C, Churazov E & Zhuravleva I, *Mon Not R Astron Soc*, 501 (2021) 1038-1045.
5 Rostilov T A & Ziborov V S, *Acta Astronaut*, 178 (2021) 900-907.
6 Figueroa-Labastida M, Luong M B, Badra J, Im H G & Farooq A, *Combust Flame*, 234 (2021) 111621.
7 Langenderfer M, Williams K, Douglas A, Rutter B & Johnson C E, *Shock Waves*, 31 (2021) 175-192.
8 Khavari M, Priyadarshi A, Hurrell A, Pericleous K, Eskin D & Tzanakis I, *J Fluid Mech*, 915 (2021) 1-22.

9 Ke L, Liu K, Sha Y, Wu G & Wang Z, *Thin-Walled Struct*, 166 (2021) 107933.
10 Zank G P et al, *Astrophys J*, 913 (2021) 127.
11 Mazrouei-Sebdani Z, Begum H, Schoenwald S, Horoshenkov K V & Malfait W J, *J Non Cryst Solids*, 562 (2021) 120770.
12 Begum H & Horoshenkov K V, *Appl Sci (Switz)*, 11 (2021) 4593.
13 Riahipour R, Nemati M S, Zadehmohamad M, Abadyan M R, Tehrani M & Baniassadi M, *Polym Polym Compos*, 30 (2022) 1-10.
14 Tang M, Wu Y, Zong H, Guo S, Liang H & Luo Y, Phys Fluids, 33 (2021) 1-12.
15 Xie Y, Zhou B & Du A, *Adv Compos Hybrid Mater*, 4 (2021) 248-256.
16 Almesmari A, Jarrar F, Almaskari F, Marpu P, Abdul Shukoor N & Govindan J, *CEAS Space* J, 13 (2021) 133-143.
17 Bottenfield B, Bond A G, English B A, Flowers G T, Dean R N & Adams M L, *IEEE Trans Compon Packag Manuf Technol*, 11 (2021) 543-556.
18 Mistry D et al, *Nat Commun*, 12 (2021) 1-10.
19 Bertarelli A, Carra F, Mariani N & Bizzaro S, Adv Tungsten Refract Hardmater IX Proc Int Conf, (2014) 486-500. 20 Patil S P, Kulkarni A & Markert B, *Comput Mater Sci*, 189 (2021) 110252.
21 Pavlov A V, Shchepanyuk T S, Chebykin E O, Skriabin A S & Telekh V D, *J Phys Conf Ser*, 2270 (2022) 012061.
22 Scapin M & Peroni L, *Metals (Basel)*, 12 (2022) 670.
23 Morena A & Peroni L, *Mater (Basel)*, 14 (2021) 7079.
24 Mayer A E, Lekanov M V, Grachyova N A & Fomin E V, *Metals (Basel)*, 12 (2022) 402.
25 Maximiano P, Durães L & Simões P, *Ind Eng Chem Res*, 58 (2019) 18905-18929.
26 Xie Q, Wen H, Ren Z, Liu H, Wang B & Wolanski P, J Loss *Prev Process Ind*, 49 (2017) 753-761.
27 Submitted T, Energy Performance Analysis and Materials Characterization of Aerogel Insulation Blankets, Thesis, (2022).
28 Hoseini A, McCague C, Andisheh-Tadbir M & Bahrami M, *Int J Heat Mass Transf*, 93 (2016) 1124-1131.
29 Lee K J, Choe Y J, Kim Y H, Lee J K & Hwang H J, *Ceram Int*, 44 (2018) 2204-2208.
30 Chakraborty S, Pisal A A, Kothari V K & Venkateswara Rao A, *Adv Mater Sci Eng*, 2016 (2016) 2495623.
31 Abaszade R G, J *Optoelectron Biomed Mater*, 14 (2022) 107-114.
32 Low I, Albetran H M & Degiorgio M, J *Nanotechnol Nanomater*, 1 (2020) 23-30.
33 Albetran H M, *J Nanomater*, 2021 (2021) 5546509.
34 Gomez C G, Linarez Pérez O E, Avalle L B & Rojas M I, *J Electroanal Chem*, 898 (2021) 115621.
35 Du A et al, *High Power Laser Sci Eng*, 9 (2021) 1-9.
36 Du A et al, *High Power Laser Sci Eng*, 9 (2021) 1-9.
37 Morton J A et al, *Mater Today*, 49 (2021) 10-22.
38 Farivar F, Lay Yap P, Karunagaran R U & Losic D, *C (Basel)*, 7 (2021) 41.